Rare-earth adatoms on GaN (0001)

Donghan Shin, Tobias Hadamek, and Alexander A. Demkov*
Department of Physics, The University of Texas at Austin, Austin, Texas 78712, USA

(Received 2 September 2018; revised manuscript received 22 March 2019; published 30 April 2019)

Several oxides, including those of rare-earth metals such as Gd_2O_3, have been used to passivate the GaN (0001) surface and are being considered as possible gate oxides in metal-oxide-semiconductor high electron mobility transistor applications. One of the problems in heteroepitaxy of rare-earth oxides (REOs) on GaN is poor wetting related to the unfavorable interface and film surface energy balance. The use of Zintl and Zintl-like intermetallic compounds can offer a solution to overcome this problem. Using density-functional theory, we investigate the bare (0001)-oriented surface of wurtzite GaN and rare-earth Eu, Gd, and Ce adatoms on it including surface mobility, wetting, and electronic structure. We also explore the possibility of forming a Zintl-like transition layer, $EuGa_2$. Our results provide a microscopic understanding of the intermetallic layer formation and its potential role in the heteroepitaxy of REOs on GaN.

DOI: 10.1103/PhysRevMaterials.3.044607

I. INTRODUCTION

As the semiconductor industry strives to further improve the performance of traditional silicon-based devices, other possible channel materials are being considered. In particular, III–V compound semiconductors have received significant attention due to their very high electron mobility [1]. After high gate leakage current ended the use of SiO_2 as a gate oxide in metal-oxide-semiconductor field-effect transistors (MOSFETs), alternative gate oxides with high dielectric permittivity, such as HfO_2, have been developed to improve device performance [2,3]. Once SiO_2 was replaced with high-permittivity (high-k) dielectrics, silicon itself no longer had to be used as the channel material. GaN is a material of choice for high-power, high-temperature, and high-frequency applications due to its large band-gap energy, high electron mobility, high saturation velocity, high breakdown field, and high operating temperature [4,5].

Many oxides have been tried in order to develop a gate dielectric for the MOS stack in a high electron mobility transistor. Ga_2O_3, a native oxide of GaN, has been proposed as a potential gate dielectric in GaN-based devices [6]. Thin-film growth of Al_2O_3 and HfO_2 on GaN using atomic layer deposition has also been reported [5,7], but these structures suffer from severe fixed charge effects [8]. Rare-earth oxides or REOs have several very attractive features such as excellent electrical and optical properties, thermal and chemical stability, wide band gaps, and relatively high dielectric constant. As a result, they have been recently studied for gate oxide applications [9–11]. Growth of several REOs on GaN has been reported including Gd_2O_3 [12–16], CeO_2 [17], La_2O_3 [18,19], YbO [20], EuO [21], Eu_2O_3 [22], Er_2O_3 [23,24], Y_2O_3 [16], and Sc_2O_3 [13,18]. There are also reports of experimental investigations of Ce and Gd metal deposition on n-type GaN (0001) that suggest the formation of rare-earth nitride layers at the interface [25,26].

Oxide-semiconductor heteroepitaxy brings a set of unique challenges [27], in particular, when ionic films are grown on covalently bonded semiconductor substrates as is the case with REOs on GaN; one needs to achieve wetting to ensure layer-by-layer growth and high crystallinity of the film. To achieve wetting, the following condition for the interface and surface energies should be satisfied:

$$\gamma_{\text{substrate}} > \gamma_{\text{film}} + \gamma_{\text{interface}}, \tag{1}$$

where $\gamma_{\text{substrate}}$, γ_{film}, and $\gamma_{\text{interface}}$, are the surface energies of the substrate and film, and the energy of the interface, respectively. For a pair of dissimilar materials like an oxide with its ionic bonding and a largely covalent semiconductor like GaN, the interface energy is likely to be rather high [27]. This makes wetting difficult to achieve. Therefore, to promote two-dimensional growth, an interlayer capable of mediating between the two different bonding types would be useful. It should have the capability to lower the energy of the interface and reduce the interface defect density. Ideally, one would need a material that can "transition" between different types of bonding. One possible class of such materials is the Zintl-Klemm intermetallics that straddle the divide between the purely covalent and metallic bonds [28]. A few atomic layers of these materials have been shown to be a promising element to engineer the wetting condition and to reduce the density of interfacial defects [29]. A Zintl-Klemm intermetallic consists of an electropositive metallic species A (alkali-, alkaline-earth-, or rare-earth-metal) and a more electronegative metallic species X (third or fourth main group element). Due to a large difference in the electronegativity, charge transfer occurs from the electropositive metal A to the electronegative metal X. Structurally, species X forms a sublattice with a covalent character typical for the isovalent element [30,31]. In the case of REO growth on GaN it is natural to take the rare-earth element (electronegativity of 1.10 to 1.29 on the Pauling scale) as the electropositive element and Ga

*Corresponding author: demkov@physics.utexas.edu

(1.81 on the Pauling scale) as the electronegative element. For example, the digallide $EuGa_2$, which has a hexagonal crystal structure and therefore is symmetry matched to the wurtzite GaN (0001) growth surface, would be a possible choice.

In order to study the feasibility of such a Zintl-Klemm interlayer based on a rare-earth metal and Ga, we investigate rare-earth adatoms on the Ga-terminated GaN (0001) surface using density-functional theory. We identify the preferred adsorption sites for Eu, Gd, and Ce and investigate the nature of charge transfer to the surface Ga. To validate our theory, we compute the surface core-level shifts (SCLS) for the Ga $3d$ semicore level in the presence of a Eu *adatom*, which can potentially be used to correlate the theoretical results with x-ray photoelectron spectroscopy (XPS) data.

II. METHODOLOGY

All calculations are performed using density-functional theory (DFT) as implemented in the Vienna *Ab initio* Simulation Package (VASP) code [32]. We employ the generalized-gradient approximation to the exchange-correlation energy functional. We use projector-augmented-wave potentials [33] to describe Ga, N, Eu, Gd, and Ce, and a cutoff energy of 600 eV is used. We employ a Hubbard U of 8.0 eV for the Eu f states, and a U of 6.0 eV for the Gd and Ce f states [34–37]. The value for Eu is chosen based on a previous study of EuO [34] that for Gd is consistent with the spectroscopic data for the bulk metal [35,36], and the choice of U for Ce is based on the recent CeO_2 and Ce_2O_3 results [37]. We consider valence electron configurations $3d^{10}4s^24p^1$ for Ga, $2s^22p^3$ for N, $5s^25p^66s^24f^7$ for Eu, $5s^25p^66s^25d^14f^7$ for Gd, and $5s^25p^66s^25d^14f^1$ for Ce. Each self-consistent electronic calculation is converged to within 10^{-6} eV per cell, and the ionic relaxation is iterated until the forces are less than 0.01 eV/Å. For the Brillouin zone integration of bulk and supercell structures, we use the $8 \times 8 \times 8$ and $6 \times 6 \times 1$ Monkhorst-Pack k-point meshes, respectively. We use an $8 \times 8 \times 1$ k-point mesh for the density of states calculation. The calculated lattice constants and internal parameter u for bulk wurtzite GaN are $a = 3.22$ Å, $c = 5.23$ Å, and $u = 0.380$. These values compare favorably with the experimental parameters, $a = 3.19$ Å, $c = 5.19$ Å, and $u = 0.377$ [38]. The calculated band gap of bulk GaN is 1.8 eV, which underestimates the experimental band gap of 3.4 eV [39]. To investigate the surface properties and adatoms on the GaN surface, we use a 14-layer-thick (2×2) GaN (0001) slab as shown in Fig. 1. Figure 1(a) shows a (0001)-oriented GaN slab. Since the (0001) orientation is polar, the top layer is Ga terminated and the bottom layer is N terminated. The N atoms in the bottom layer are saturated by pseudohydrogen atoms. Figure 1(b) shows sites available for the adatoms to bond on the GaN surface. T1 represents the site over the Ga atom and T4 represents the site over the N atom. We distinguish T4 and T4* (alongside the a axis) and deal with these as different sites in a (2×2) lateral cell. H3 represents the hollow site at the center of the cell.

III. RESULTS AND DISCUSSION

We start our investigation by computing the electronic structure of a bare Ga-terminated and Ga-polar GaN (0001) surface. First, we calculate the electronic structure without atomic relaxation. From the layer-by-layer orbital-projected density of states (pDOS) shown in Fig. 2(a), we note that in-gap surface states are induced and the Fermi level crosses the surface band, indicating a metallic surface. Deeper in the bulklike layers of the slab, the surface states disappear. These surface states have predominantly s- and p-like character in the Ga surface layer. In the next N surface layer, the surface states are derived from the p orbital. This is consistent with previously reported DFT calculations [40]. If we allow for atomic relaxation, both the electronic and atomic structures are found to be different. In Fig. 2(b), the pDOS of a (2×2) fully relaxed GaN (0001) slab is shown. Now the surface band is split into two: the lower subband containing the Fermi level and the upper subband about 1.0 eV above the Fermi level. The pDOS suggests that the states around the Fermi level are mainly derived from the s orbitals, whereas the states above the Fermi level are mainly composed of the p orbitals. We also see a geometric change in the atomic structure [Fig. 2(c)]. As the surface layers relax, two Ga atoms of the (2×2) surface

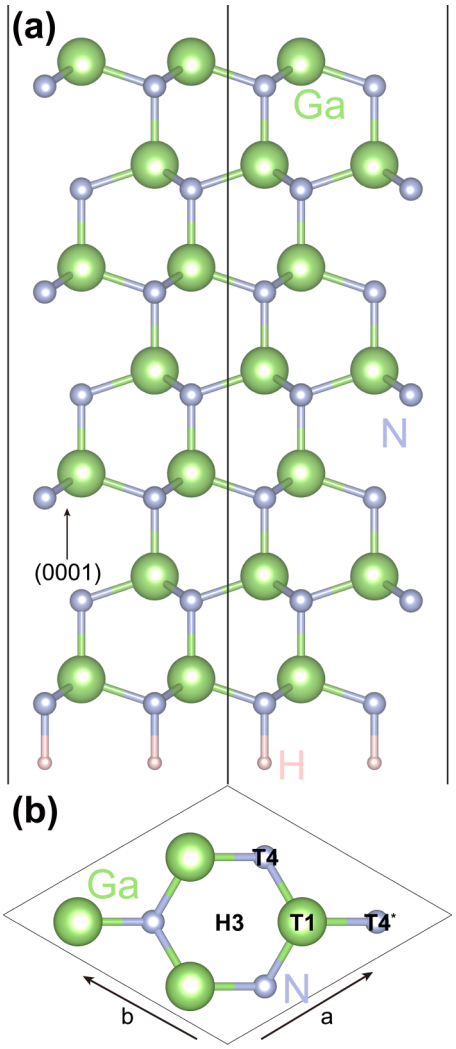

FIG. 1. (a) Side view of ideal slab of GaN (0001). (b) Top view of the GaN (0001) surface. T1, T4, and H3 are site on Ga atom, site on N atom, and hollow site, respectively.

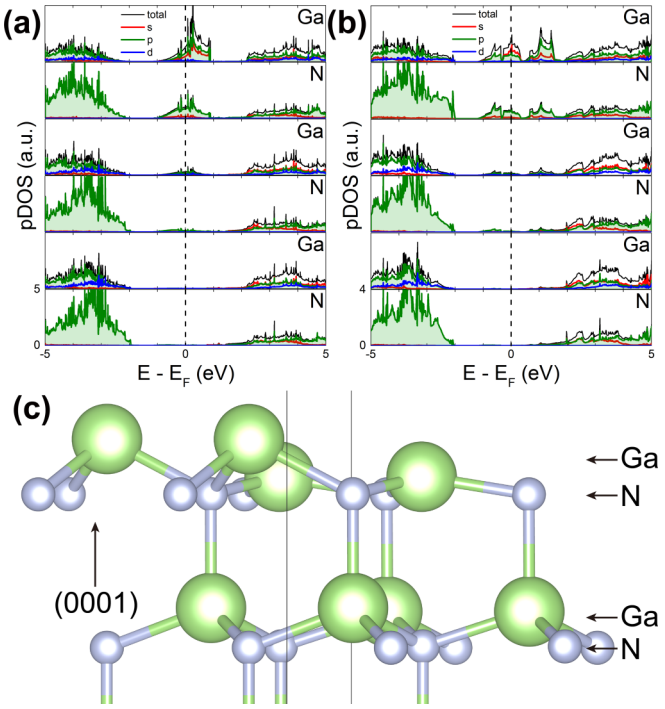

FIG. 2. (a) Layer-by-layer orbital-projected DOS (pDOS) of the bare (2×2) GaN (0001) surface without relaxation and (b) after relaxation. Only top six layers are shown. (c) Atomic structure of GaN (0001) after relaxation.

cell are pushed down, while the other two Ga atoms move vertically to a higher position. Looking at the pDOS, we note that the metallic states around the Fermi level originate from the "up Ga" atoms. In contrast, the empty states above the Fermi level are related to the "down-Ga" atoms. The surface band splits into two and charge transfers to a low-energy *s*-like band from a high-energy *p*-like band, similar to what happens on (2×1)-reconstructed Si and Ge (001) surfaces [41]. However, due to the electron count specific to a III–V semiconductor, there is no true Peierls transition and the surface remains metallic, although the emergence of pseudogap is clearly seen 0.4 eV above the Fermi level.

We now look at what happens as rare-earth (RE) adatoms are placed on the GaN (0001) surface First, we compute the potential energy surface (PES) for each of the three rare-earth adatoms considered, which is shown in Fig. 3. To compute the PES, we consider a (6×6) grid over the surface cell, and calculate the total energy placing rare-earth adatoms on that grid, fixing their lateral movement (all other atomic coordinates are optimized). The spatial resolution is 1.29 Å and the energy values between the grid points are obtained by spline interpolation. The PES for a Eu adatom [Fig. 3(a)] suggests that Eu binds preferentially to N (site T4), while Ga repels it. The potential energy difference between the T4 (over N) and T1 (over Ga) sites is 0.6 eV. We also see that the hollow site H3 provides a deep potential well comparable in stability with the lowest-energy site T4. From the PES for a Gd adatom [Fig. 3(b)], we can see behavior very similar to that of Eu, in which the Ga atoms repel Gd, while N offers a stable bonding site. The potential-energy difference between the T4 (over N) and T1 (over Ga) sites is larger, 1.5 eV, in the Gd case. The potential energy is also low at the hollow site H3, but is higher than at T4. The PES for a Ce adatom [Fig. 3(c)] is similar to that of Eu and Gd adatoms. The potential energy is lowest at T4* (above N) site, while the energy of the site above the Ga atoms is about 1.4 eV higher than the energy of T4*. It is worth noting that Gd and Ce adatoms have a larger energy difference between the T4 and T1 sites than a Eu adatom. To estimate the timescale of adatom surface diffusion, one can use a simple Arrhenius formula for kinetics, $1/\tau = \nu e^{-E/k_B T}$, where τ is a time interval between adatom hops, E is the energy barrier, and ν is an attempt frequency ($\nu \approx 10^{12}\ \mathrm{s}^{-1}$). We performed a transition-state analysis using the climbing nudged elastic band (cNEB) method [42,43] to find the migration barriers for the diffusion path from T4 to H3 (Fig. 4). For a path taking Eu from T4 (over nitrogen) to H3 (hollow site), the barrier is estimated to be only 0.3 eV and the timescales are on the order of 10^{-7} s and 10^{-11} s at room temperature and 750 °C, respectively [Figs. 4(a) and 4(b)]. On the other hand, for Gd and Ce atoms, along the path from T4 to H3 the barrier is 0.6 eV

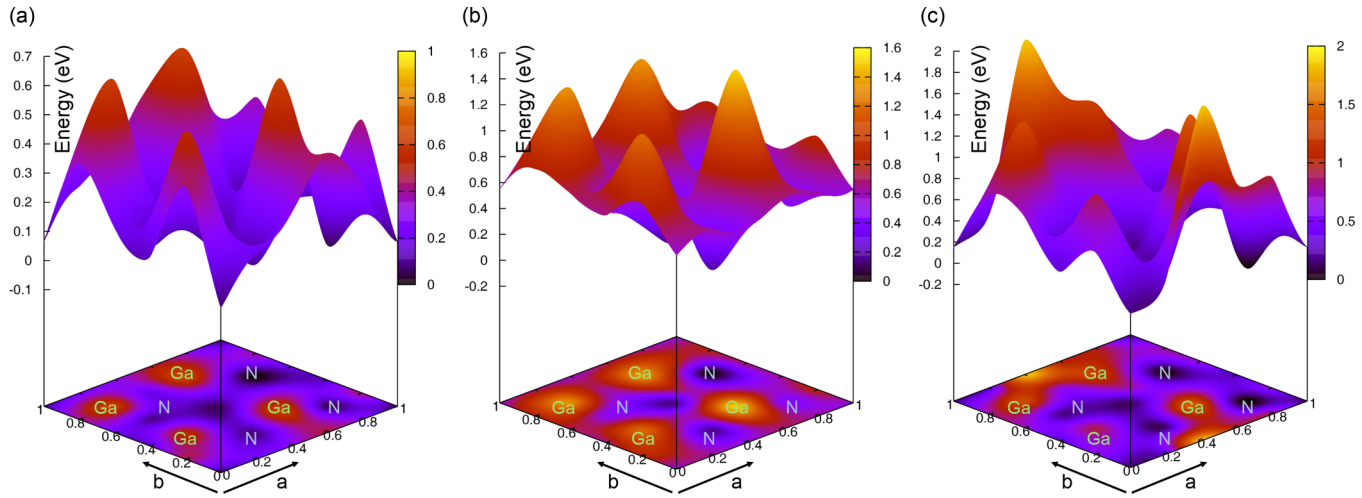

FIG. 3. Potential energy surface (PES) plot for (a) Eu adatom on GaN(0001), (b) Gd adatom on GaN (0001), and (c) Ce adatom on GaN (0001). The energy of the lowest-energy configuration sets zero of the energy scale.

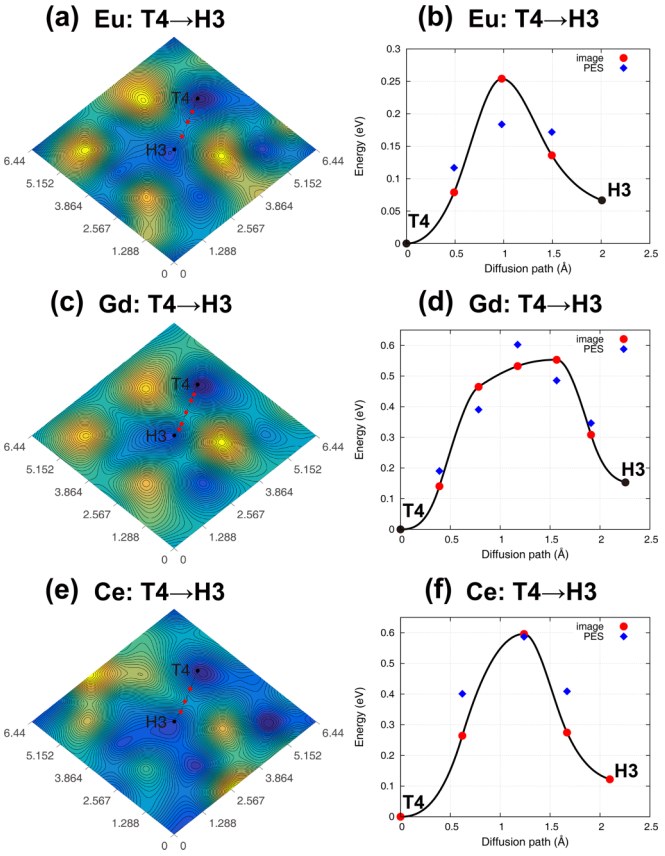

FIG. 4. Diffusion path from T4 to H3 of the rare-earth adatoms on the GaN surface: (a) Eu, (c) Gd, and (e) Ce. The line separation of the contour plot is 13, 30, and 38 meV for (a), (c), and (e), respectively. Black dots represent the initial and final points of the path and red dots represent the images in cNEB calculations. Migration barrier estimated by cNEB calculation for (b) Eu adatom, (d) Gd adatom, and (f) Ce adatom. For comparison, PES data at the image positions are plotted with blue points.

and diffusion times are on the order of 10^{-2} s and 10^{-10} s at room temperature and 750 °C, respectively [Figs. 4(c)–4(f)]. This suggests that Eu adatoms are much more mobile on the GaN (0001) surface than Gd and Ce, which is consistent with the aforementioned PES investigation. Overlaying the cNEB-calculated reaction path over the contour plot of the PES [Figs. 4(a), 4(c), and 4(e)], we see that the path from T4 to H3 is close to a straight line between the two potential wells. In Figs. 4(b), 4(d), and 4(f) we compare the energy barriers along the path computed using the cNEB method and estimated from the PES. Overall, the agreement is excellent. Minor discrepancies are related to the interpolated nature of the PES and a relatively small number of images in the cNEB calculations.

We now analyze the geometric changes of the surface atomic structure as we place rare-earth adatoms on GaN. From the PES, the adatoms can be placed on either H3 (hollow) or T4 (over N) sites [see Fig. 1(b)]. As we place the rare-earth adatoms, three surface Ga atoms adjacent to it are displaced upwards by 0.35 Å along the (0001) direction, whereas the Ga furthest away from the adatom moves 0.31 Å down. As an example of such relaxation, the atomic structure for the Ce adatom adsorbed at two different sites on GaN (0001) is shown in Figs. 5(a) and 5(b). For Ce at the H3 site, the atomic distances between Ce and adjacent Ga atoms are 3.00, 3.03, and 2.96 Å. For Ce at the T4 site, the distances between Ce and Ga are 2.96, 2.96, and 2.97 Å. For Eu on GaN, the atomic distances between Eu and Ga are 3.27, 3.07, and 3.12 Å for the H3 site, and 3.04, 3.05, and 3.24 Å for the T4 site. For Gd at the H3 site, the distances between Gd and adjacent Ga atoms are estimated to be 2.88, 2.95, and 2.91 Å. For Gd at the T4 site, the distances between Gd and adjacent Ga atoms are 2.87, 2.88, and 2.88 Å. These interatomic distances are comparable with the RE–Ga bond lengths in AlB_2-type (space group $P6/mmm$) rare-earth digallides [Fig. 5(c)]. The rare-earth atom to gallium bond lengths in the digallides are 3.31 Å for $CeGa_2$ [44], 3.37 Å for $EuGa_2$ [45], and 3.2 Å for $GdGa_2$ [46].

As rare-earth metal deposition during REO growth typically occurs at relatively high temperature, especially using molecular-beam epitaxy (>750 °C) [22,25,26], surface reactions are a strong possibility. To get some idea of the surface reactivity of rare-earth metals, we consider the exchange of the rare-earth metal atom with a surface Ga resulting in a "flip" structure. To build the flip structure, we exchange the positions of the RE adatoms and one Ga atom at the surface, then we relax the atomic positions. After atomic relaxation, we compare the total energy of the flip structure with that of the normal structure (without exchange of positions). Interestingly, there is an energy gain for all three rare-earth metals considered here. The energies of the flip structures are lowered by 1.02, 2.15, and 1.62 eV for Eu, Gd, and Ce adatoms, respectively, with respect to the initial adatom configurations. When placing rare-earth metals in the second subsurface Ga layer we find no further energy gain compared with the flip structures. We calculate the migration barrier between the normal and flip structures for the Ce adatom using the cNEB method. The barrier is estimated to be 1.7 eV

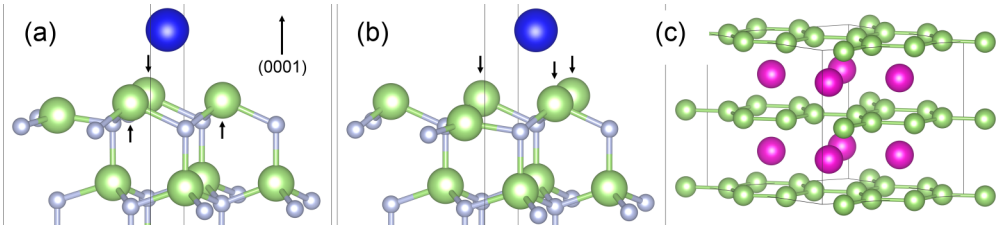

FIG. 5. (a) Atomic structure of Ce adatom on H3 site at GaN (0001). (b) Atomic structure of Ce adatom on T4 site at GaN (0001). (c) Crystal structure of AlB_2-type hexagonal $EuGa_2$. Blue, light green, and magenta represent Ce, Ga, and Eu, respectively.

and the diffusion time is on the order of 10^{16} s and 10^{-4} s at room temperature and 750 °C, respectively. This suggests that rare-earth metals are likely to react with the surface if they are deposited on GaN (0001) at high temperature. Our results are consistent with previous DFT investigations of the GaN surface with replacement by other rare-earth atoms [47,48]. The simulation cell size is generally a concern as the larger the area of the simulation cell, the more configurations are possible. To examine dependence of simulation cell size, we have performed the same calculations using a larger (3×3) GaN surface. As we compare the total energy of Eu adatom placed above N and the flip configuration, the total energy of the flip configuration is lower than that of Eu adatom atop N. So in this respect, the results do not depend on the size of the surface simulation cell.

XPS is a commonly used tool in analyzing the physics and chemistry of a surface. It is a very surface-sensitive technique due to the small (few nanometer) escape depths of the photoelectrons. XPS core-level positions can reveal information about chemical bonding. On the very surface the chemical and structural bonding environment is slightly different from the bulk and often surface core-level shifts can be observed. The interpretation of the magnitude and direction of the SCLS can be facilitated by *ab initio* theory. In a photoemission process one core hole is created at a particular atom. In response to the created core hole the system screens this positive charge and the relaxation energy due to screening can be captured using the final-state theory. A particular core-level binding energy in the final state theory is calculated by taking the total energy difference between the ground-state energy and energy of the system with a core hole [49,50]:

$$E_B^{\text{final}} = E'(n_c - 1) - E(n_c), \tag{2}$$

where $E(n_c)$ is the total energy of ground state and $E'(n_c - 1)$ is the total energy of the system with a core hole. In the DFT calculation, the single electron is removed from the core level and is placed into a valence level by generating a pseudopotential with a core hole. An extra electron is added to the calculation to ensure the overall charge neutrality of the system [51]. Taking the difference between the binding energy of surface and bulk atoms, the SCLS can be estimated. To gain further insight into the electronic structure and provide validation of our models, we calculate the SCLS of the Ga $3d$ core level and valence charge density corresponding to occupied states with and without atomic relaxation. In the geometrically optimized structure of bare GaN (0001), the SCLS is estimated to be -2.17 and -0.46 eV for the up- and down Ga atoms, respectively. This indicates that the $3d$ core-level binding energy of the Ga atoms at the surface is lower than the atoms in the bulk, with a 1.71 eV difference in the binding energies between the two kinds of surface atoms. This is consistent with angle resolved XPS measurements which shows lower binding energies for atoms closer to the surface [52]. Initially, without atomic relaxation, the charge is mostly distributed around the Ga and N atoms at the surface [Fig. 6(a)]. The shape of the charge distribution is consistent with hybridization of s and p_z orbitals and this is confirmed by our pDOS analysis. After atomic relaxation, however, the charge distribution is found to be different [Fig. 6(b)]. The

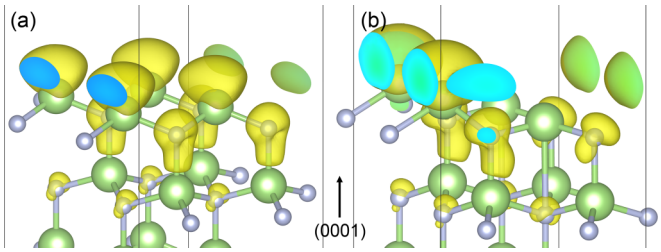

FIG. 6. Partial charge density corresponding to the occupied states in bare GaN slab (a) before relaxation and (b) after relaxation. Saturation level is set to (a) 0.0026 $e/\text{Å}^3$ and (b) 0.004 $e/\text{Å}^3$.

charge is only distributed around the upper Ga atoms at the surface and the lower Ga atoms do not show a significant contribution. This suggests that a charge transfer from the lower to the upper Ga atoms occurs in order to occupy low-energy states. The binding energy of the $3d$ core level at the higher charge density atoms (upper Ga) is shifted more in binding energy towards vacuum due to Coulomb repulsion.

We also investigate the effect of Eu on the electronic structure of the GaN (0001) surface. In Fig. 7(a), the calculated SCLS of the Ga $3d$ core level with a Eu adatom is shown. Here the Ga atoms closer to Eu (Ga1 and 2) have lower binding energy than the Ga atom far from Eu (Ga3). The binding energy shift is around -2 eV for these atoms. The binding energy of Ga3 is lower than that of Ga in the

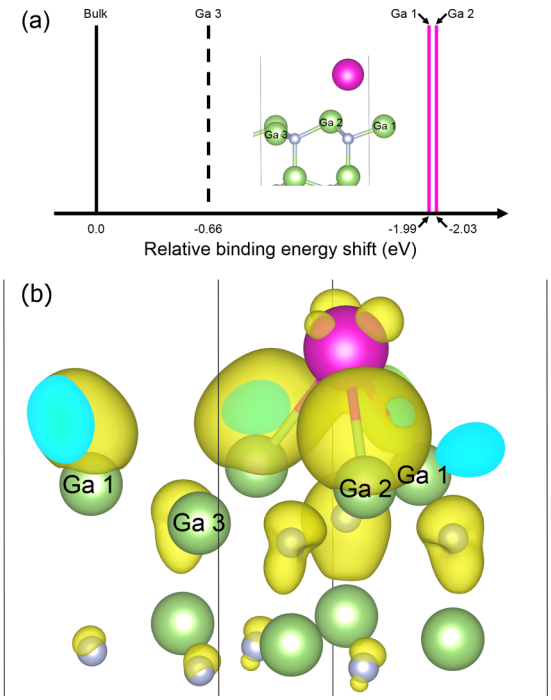

FIG. 7. (a) Ga $3d$ chemical shifts for different Ga surface atoms with respect to that in bulk Ga calculated using final-state theory. Insets are the atomic structure of 3 Ga atoms in the GaN surface. (b) Partial charge density corresponding to occupied states in the GaN surface with Eu adatom. Saturation level is set to 0.005 $e/\text{Å}^3$. Magenta, light green, and light gray represent Eu, Ga, and N atoms, respectively.

bulk, which is similar to the results obtained for the bare GaN surface. The binding energy reduction of 0.66 eV is also comparable with that of the bare surface (0.45 eV). To clarify this difference, we calculate the corresponding charge density of the GaN surface with a Eu adatom which is shown in Fig. 7(b). Charge is distributed between the Eu atom and three adjacent Ga atoms, which indicates that there is chemical bonding between Eu and Ga. There is no significant charge present around the Ga atom far away from Eu. As there is charge transfer to the Ga atoms bonded with the Eu atom, the Ga $3d$ core level has lower binding energy in the presence of RE.

To gain further insight into charge transfer between the rare-earth adatoms and the Ga-terminated surface, we perform Bader charge and model Hamiltonian analysis. According to our Bader charge calculation, charge is lost by the RE adatoms and gained by Ga atoms at the surface, which indeed suggests Zintl-like charge transfer from the electropositive rare-earth to the more electronegative Ga. We introduce a simple tight-binding two-level Hamiltonian to illustrate this effect. Taking two basis states, one from the rare-earth atom and one from Ga: $|\mathrm{RE}\rangle$ = rare-earth, $|\mathrm{Ga}\rangle$ =, with corresponding energies E_A, E_B ($E_A > E_B$), we construct a tight-binding model:

$$\begin{pmatrix} E_A & \beta \\ \beta^* & E_B \end{pmatrix}, \tag{3}$$

where β is a hopping parameter between the two sites. To illustrate the charge transfer, we compute the ratio of the wave-function coefficients C_A^2/C_B^2 as a function of two parameters of the model, $\Delta = (E_A - E_B)/2$ and β. The ratio of the wave-function coefficients is given by

$$\frac{C_A^2}{C_B^2} = \frac{1}{1 + 2x^2 + 2x(1+x^2)^{1/2}}, \tag{4}$$

where x is Δ/β. As $x \to 0$, the ratio approaches 1, which means no charge transfer between RE and Ga sites. For large x, the ratio approaches zero, which means all charge in RE site is transferred to the Ga site. This suggests that there is more charge transfer when x is large, corresponding to a large energy difference and a small hopping parameter. We assume that the energy difference between the rare-earth site and Ga site is proportional to the difference of electronegativity (δ) and the hopping parameter is related to the overlap integral and is a function of $1/d^2$, where d is the distance between the two sites. Thus, x is proportional to the product δd^2. The atomic distance can be estimated from the DFT calculation, employing experimental data, or simply as a sum of covalent radii. We summarize parameters of the model in Table I along with the Bader charge analysis. Bader charge analysis suggests that the greatest amount of charge transfer occurs for the Gd adatom while the least amount of charge transfer occurs for Eu. In our simple model, δd^2 is largest for the Ce adatom and δd^2 is smallest for the Gd adatom. Comparing the simple model with the Bader analysis, they are consistent when considering Ce and Eu adatoms but there is a discrepancy in the case of Gd. Indeed, Gd is unusual among the RE metals owing to its occupation of the $5d$ shell instead of the f shell.

Another question to consider is whether there is a specific RE coverage resulting in a more stable surface

TABLE I. Parameters used in a model Hamiltonian analysis and Bader charge analysis results.

Adatom	Ce	Eu	Gd
Electronegativity (χ)	1.12	1.2	1.2
δ ($\chi_{\mathrm{Ga}} - \chi_{\mathrm{RE}}$)	0.69	0.61	0.61
RE-Ga distance (Å) (DFT)	2.96	3.11	2.88
RE-Ga distance (Å) (exp.) [44–46]	3.31	3.37	3.20
Covalent radius (Å)	2.04	1.98	1.96
RE-Ga distance (Å) (covalent radius)	3.26	3.2	3.18
δd^2 (DFT)	6.06	5.91	5.05
δd^2 (exp.)	7.54	6.95	6.25
δd^2 (covalent radius)	7.33	6.25	6.17
Bader analysis			
Loss of charge in RE	0.86 e^-	0.83 e^-	0.90 e^-
Gain of charge by Ga in the surface layer	0.89 e^-	0.86 e^-	0.94 e^-

configuration. To rationalize the stable coverage, one could invoke the electron-counting argument. Since Ga has three valence electrons and is fourfold coordinated in wurtzite GaN, each Ga bond has a fractional number of electrons (0.75 e^-). There are four Ga dangling bonds in a (2×2) surface cell, thus the surface needs four electrons to have half filling. Since the four dangling bonds already have three electrons, the surface needs only one additional electron to achieve this. Consider for example, Eu coverage of quarter- and half monolayer (ML). We calculate the adsorption energy for each coverage and perform the Bader charge analysis. The adsorption energy is given by

$$E^{\mathrm{adsorption}} = \frac{1}{2A}\left(E(\mathrm{slab}) - E_{\mathrm{bare}}(\mathrm{slab}) - N_{\mathrm{Eu}}\left(\mu_{\mathrm{Eu}} + E_{\mathrm{Eu}}^{\mathrm{bulk}}\right)\right), \tag{5}$$

where A is the simulation cell area, E(slab) is the total energy of the GaN slab with Eu adatom under consideration, E_{bare}(slab) is the total energy of the bare GaN slab, and N_{Eu} is the number of Eu atoms added. The chemical potential for Eu, μ_{Eu}, is referenced to bulk energy of Eu metal. We assume $EuGa_2$ to be the first phase to appear (it has the lowest formation energy among the possible compounds), which limits the chemical potentials of Eu and Ga via the following equilibrium condition:

$$\mu_{\mathrm{Eu}} + 2\mu_{\mathrm{Ga}} = \Delta_f^{\mathrm{EuGa_2}}, \tag{6}$$

where $\Delta_f^{\mathrm{EuGa_2}} \equiv E_{\mathrm{EuGa_2}}^{\mathrm{bulk}} - E_{\mathrm{Eu}}^{\mathrm{bulk}} - 2E_{\mathrm{Ga}}^{\mathrm{bulk}}$ is the formation energy of $EuGa_2$ bulk metal. Assuming Ga-rich condition ($\mu_{\mathrm{Ga}} = 0$), we have a range of μ_{Eu} in Eq. (2):

$$\Delta_f^{\mathrm{EuGa_2}} \leqslant \mu_{\mathrm{Eu}} \leqslant 0. \tag{7}$$

This adsorption energy calculation, dashed lines shown in Fig. 8, suggests that a half ML of Eu on the surface is more stable under the Eu-rich conditions. The DOS indicates that the surface is insulating with a small gap of about 10 meV. Recall that after relaxation of the bare GaN surface, the surface band is almost split into two subbands and there is a Peierls-like pseudogap between them, as shown in Fig. 2(b). However, due to the odd valence of gallium, the lower subband is not fully occupied rendering the surface metallic. As we place Eu

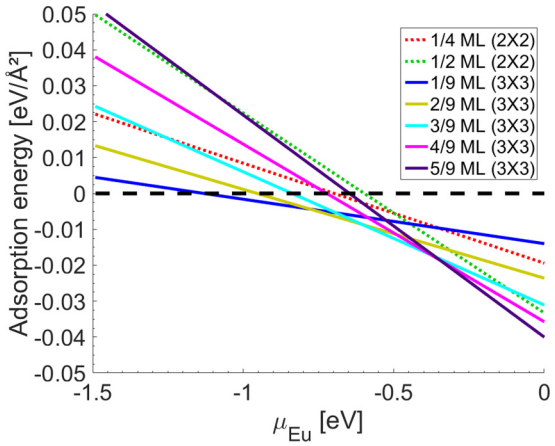

FIG. 8. Adsorption energy for Eu on GaN (0001) for different Eu coverage as a function of Eu chemical potential, μ_{Eu}. The results are shown for a (2×2) and larger (3×3) simulation cells. The range of the chemical potential is set by the equilibrium conditions corresponding to forming the Eu metal ($\mu_{\mathrm{Eu}} = 0\,\mathrm{eV}$, Eu rich) or $EuGa_2$ ($\mu_{\mathrm{Eu}} = -1.49\,\mathrm{eV}$, Eu poor) intermetallic at the surface.

adatoms on the surface, there is a Zintl-like charge transfer and the electrons fill the lower subband. The additional surface relaxation and the presence of $Eu^{+\delta}$ result in the surface becoming insulating (the pseudogap becomes a real gap). From the DOS of the relaxed bare surface we estimate the number of electrons that is needed to fill the lower subband to be approximately $1.2\,e^-$ ([for the (2×2) cell]. The Bader charge analysis of the structure with only one added Eu suggests that the transferred charge is about $0.8\,e^-$. Therefore, to fill the lower surface subband, we need more than one Eu atom. What is interesting here is that the height of Eu above the surface controls the amount of charge transferred, and for two Eu adatoms on a (2×2) cell the surface receives the right amount of charge to make it insulating. Indeed, as we place two Eu atoms on the surface, the Bader analysis confirms that there is charge transfer of $1.2\,e^-$. This is surprisingly similar to what happens for half monolayer of Sr on Si (001) [29,53]. We have also calculated the adsorption energy for several Eu coverages on the (3×3) surface cell. The situation is a little bit more complicated for a (3×3) cell due to the odd multiplier. However, under the Eu-rich conditions, the Eu coverage close to half monolayer is again the most stable (solid lines in Fig. 8). There is a difference when comparing the energy as a function of coverage, mostly due to the difference in the electron count as discussed above.

IV. CONCLUSIONS

Using density-functional theory, we investigated theoretically the electronic and atomic structure of the bare Ga-polar Ga-terminated GaN (0001) surface. We focus on the effect of rare-earth adatoms (Ce, Eu, Gd) on the electronic structure and geometry of the surface. The transition-state calculations suggest that the Eu adatom is more mobile on the surface than Gd and Ce adatoms. We also find a low migration barrier for swapping a rare-earth adatom with a surface Ga atom, indicating that there is a strong possibility for the reaction between the rare-earth adatoms and the surface to form rare-earth nitrides. From the surface core-level shift and charge-density analysis, we find that there is Zintl-like charge transfer from RE metal to Ga as it is placed on the GaN surface. Due to this charge transfer, the GaN surface undergoes a geometric and electronic relaxation. For example, the atomic and electronic structures of the GaN surface with Eu are reminiscent of that of Zintl intermetallic $EuGa_2$. Such Zintl-like surface templates can potentially reduce the interface energy in the heteroepitaxy of rare-earth oxides on GaN (0001). We find that in the case of Eu, approximately half-monolayer coverage is most stable resulting in an insulating surface. This can be understood considering electron counting. What is unusual is that the amount of charge transferred to the surface is controlled by the height of Eu adatoms above it. For the half-monolayer case, the height self-adjusts so the surface receives the appropriate amount of charge to become insulating.

ACKNOWLEDGMENTS

We thank Agham Posadas for critically reading the manuscript and John Ekerdt and Pei-Yu Chen for many helpful discussions. The work was supported in part by the National Science Foundation under Grant No. DMR-1507970.

[1] J. A. del Alamo, Nature (London) **479**, 317 (2011).
[2] S.-H. Lo, D. A. Buchanan, Y. Taur, and W. Wang, IEEE Electron Device Lett. **18**, 209 (1997).
[3] D. J. Frank, R. H. Dennard, E. Nowak, P. M. Solomon, Y. Taur, and H.-S. P. Wong, Proc. IEEE **89**, 259 (2001).
[4] X. Liu, H.-C. Chin, L. S. Tan, and Y.-C. Yeo, IEEE Electron Device Lett. **31**, 8 (2010).
[5] J. Yang, B. S. Eller, C. Zhu, C. England, and R. J. Nemanich, J. Appl. Phys. **112**, 053710 (2012).
[6] H. S. Oon and K. Y. Cheong, Mater. Sci. Semicond. Process. **16**, 1217 (2013).
[7] M. Ťapajna and J. Kuzmík, Appl. Phys. Lett. **100**, 113509 (2012).
[8] J. Son, V. Chobpattana, B. M. McSkimming, and S. Stemmer, Appl. Phys. Lett. **101**, 102905 (2012).
[9] G.-Y. Adachi and N. Imanaka, Chem. Rev. **98**, 1479 (1998).
[10] W. C. Chin, K. Y. Cheong, and Z. Hassan, Mater. Sci. Semicond. Process. **13**, 303 (2010).
[11] R. Dargis, A. Clark, F. Erdem Arkun, T. Grinys, R. Tomasiunas, A. O'Hara, and A. A. Demkov, J. Vac. Sci. Technol., A **32**, 041506 (2014).
[12] J. W. Johnson, B. Luo, F. Ren, B. P. Gila, W. Krishnamoorthy, C. R. Abernathy, S. J. Pearton, J. I. Chyi, T. E. Nee, C. M. Lee, and C. C. Chuo, Appl. Phys. Lett. **77**, 3230 (2000).
[13] B. P. Gila, J. W. Johnson, R. Mehandru, B. Luo, A. H. Onstine, K. K. Allums, V. Krishnamoorthy, S. Bates, C. R. Abernathy, F. Ren, and S. J. Pearton, Phys. Status Solidi A **188**, 239 (2001).
[14] M. Hong, J. Kwo, S. N. G. Chu, J. P. Mannaerts, A. R. Kortan, H. M. Ng, A. Y. Cho, K. A. Anselm, C. M. Lee, and J. I. Chyi, J. Vac. Sci. Technol., B **20**, 1274 (2002).

[15] W. H. Chang, C. H. Lee, P. Chang, Y. C. Chang, Y. J. Lee, J. Kwo, C. C. Tsai, J. M. Hong, C. H. Hsu, and M. Hong, J. Cryst. Growth **311**, 2183 (2009).
[16] W.-H. Chang, S.-Y. Wu, C.-H. Lee, T.-Y. Lai, Y.-J. Lee, P. Chang, C.-H. Hsu, T.-S. Huang, J. R. Kwo, and M. Hong, ACS Appl. Mater. Interfaces **5**, 1436 (2013).
[17] H. J. Quah, W. F. Lim, K. Y. Cheong, Z. Hassan, and Z. Lockman, J. Cryst. Growth **326**, 2 (2011).
[18] J. S. Jur, V. D. Wheeler, D. J. Lichtenwalner, J.-P. Maria, and M. A. L. Johnson, Appl. Phys. Lett. **98**, 042902 (2011).
[19] J. F. Ihlefeld, M. Brumbach, and S. Atcitty, Appl. Phys. Lett. **102**, 162903 (2013).
[20] M. D. Losego and J.-P. Maria, J. Vac. Sci. Technol., B **24**, 2110 (2006).
[21] A. Schmehl, V. Vaithyanathan, A. Herrnberger, S. Thiel, C. Richter, M. Liberati, T. Heeg, M. Röckerath, L. F. Kourkoutis, S. Mühlbauer, P. Böni, D. A. Muller, Y. Barash, J. Schubert, Y. Idzerda, J. Mannhart, and D. G. Schlom, Nat. Mater. **6**, 882 (2007).
[22] T. Hadamek, D. Shin, A. B. Posadas, A. A. Demkov, S. Kwon, Q. Wang, and M. Kim, Appl. Phys. Lett. **111**, 142901 (2017).
[23] R. M. Lin, F. C. Chu, A. Das, S. Y. Liao, S. T. Chou, and L. B. Chang, Thin Solid Films **544**, 526 (2013).
[24] P. Y. Chen, A. B. Posadas, S. Kwon, Q. Wang, M. J. Kim, A. A. Demkov, and J. G. Ekerdt, J. Appl. Phys. **122**, 215302 (2017).
[25] W. Xiao, Q. Guo, Q. Xue, and E. G. Wang, J. Appl. Phys. **94**, 4847 (2003).
[26] W. Xiao, Q. Guo, and E. G. Wang, J. Appl. Phys. **95**, 943 (2004).
[27] A. A. Demkov and A. B. Posadas, *Integration of Functional Oxides with Semiconductors* (Springer, New York, 2014).
[28] E. Zintl and W. Dullenkopf, Z. Phys. Chem. B **16**, 195 (1932).
[29] A. A. Demkov, H. Seo, X. Zhang, and J. Ramdani, Appl. Phys. Lett. **100**, 071602 (2012).
[30] A. Slepko and A. A. Demkov, Phys. Rev. B **85**, 195462 (2012).
[31] H. Seo, M. Choi, A. B. Posadas, R. C. Hatch, and A. A. Demkov, J. Vac. Sci. Technol., B **31**, 04D107 (2013).
[32] G. Kresse and J. Furthmüller, Phys. Rev. B **54**, 11169 (1996).
[33] P. E. Blöchl, Phys. Rev. B **50**, 17953 (1994).
[34] J. Lee, N. Sai, and A. A. Demkov, Phys. Rev. B **82**, 235305 (2010).
[35] B. N. Harmon, V. P. Antropov, A. I. Liechtenstein, I. V. Solovyev, and V. I. Anisimov, J. Phys. Chem. Solids **56**, 1521 (1995).
[36] L. Liu, P. Y. Yu, Z. Ma, and S. S. Mao, Phys. Rev. Lett. **100**, 127203 (2008).
[37] D. A. Andersson, S. I. Simak, B. Johansson, I. A. Abrikosov, and N. V. Skorodumova, Phys. Rev. B **75**, 035109 (2007).
[38] H. Neumann, Cryst. Res. Technol. **30**, 910 (1995).
[39] V. M. Bermudez, Surf. Sci. Rep. **72**, 147 (2017).
[40] M. Himmerlich, L. Lymperakis, R. Gutt, P. Lorenz, J. Neugebauer, and S. Krischok, Phys. Rev. B **88**, 125304 (2013).
[41] A. A. Demkov and X. Zhang, J. Appl. Phys. **103**, 103710 (2008).
[42] G. Henkelman, B. P. Uberuaga, and H. Jónsson, J. Chem. Phys. **113**, 9901 (2000).
[43] G. Henkelman and H. Jónsson, J. Chem. Phys. **113**, 9978 (2000).
[44] Entry 527126 in Pearson's Crystal Data: Crystal Structure Database for Inorganic Compounds (on DVD), Materials Park, Ohio, 2015/2016.
[45] Entry 526548 in Pearson's Crystal Data: Crystal Structure Database for Inorganic Compounds (on DVD), Materials Park, Ohio, 2015/2016.
[46] Entry 1616639 in Pearson's Crystal Data: Crystal Structure Database for Inorganic Compounds (on DVD), Materials Park, Ohio, 2015/2016.
[47] J. Guerrero-Sánchez, G. H. Cocoletzi, J. F. Rivas-Silva, and N. Takeuchi, Appl. Surf. Sci. **268**, 16 (2013).
[48] J. Guerrero-Sánchez, G. H. Cocoletzi, J. F. Rivas-Silva, and N. Takeuchi, Comput. Mater. Sci. **106**, 155 (2015).
[49] E. Pehlke and M. Scheffler, Phys. Rev. Lett. **71**, 2338 (1993).
[50] S. Lizzit, A. Baraldi, A. Groso, K. Reuter, M. V. Ganduglia-Pirovano, C. Stampfl, M. Scheffler, M. Stichler, C. Keller, W. Wurth, and D. Menzel, Phys. Rev. B **63**, 205419 (2001).
[51] L. Köhler and G. Kresse, Phys. Rev. B **70**, 165405 (2004).
[52] M. Mishra, T. C. S. Krishna, N. Aggarwal, and G. Gupta, Appl. Surf. Sci. **345**, 440 (2015).
[53] K. D. Fredrickson, H. Seo, and A. A. Demkov, J. Appl. Phys. **120**, 065301 (2016).